The Astrophysical Journal, 700:L47–L50, 2009 July 20 doi:10.1088/0004-637X/700/1/L47

VERY HIGH EFFICIENCY PHOTOSPHERIC EMISSION IN LONG-DURATION γ-RAY BURSTS

Davide Lazzati[1,2], Brian J. Morsony[2,3], and Mitchell C. Begelman[2,4]
[1] Department of Physics, NC State University, 2401 Stinson Drive, Raleigh, NC 27695-8202, USA; davide_lazzati@ncsu.edu
[2] JILA, University of Colorado, 440 UCB, Boulder, CO 80309-0440, USA
[3] Department of Astronomy, University of Wisconsin-Madison, 5534 Sterling Hall, 475 North Charter Street, Madison, WI 53706-1582, USA
[4] Department of Astrophysical and Planetary Sciences, University of Colorado, 389 UCB, Boulder, CO 80309-0389, USA
Received 2009 April 17; accepted 2009 June 11; published 2009 July 2

ABSTRACT

We numerically analyze the evolution of a long-duration gamma-ray burst jet as it leaves the progenitor star and propagates to the photospheric radius, where radiation can be released. We find that the interaction of the relativistic material with the progenitor star has influences well beyond the stellar surface. Tangential collimation shocks are observed throughout the jet evolution, out to about 100 stellar radii, which is the whole range of our simulation. We find that the jet is internally hot at the photospheric radius and we compute the photospheric emission. The photosphere is a very efficient radiator, capable of converting more than half of the total energy of the jet into radiation. We show that bright photospheres are a common feature of jets born inside massive progenitor stars and that this effect can explain the high radiative efficiency observed in long-duration bursts.

Key words: gamma rays: bursts – hydrodynamics – methods: numerical – radiation mechanisms: thermal – relativity

1. INTRODUCTION

Long-duration gamma-ray bursts (GRBs) are believed to arise when a very massive star collapses to a black hole, powering a hyper-relativistic outflow (Woosley 1993; Hjorth et al. 2003; Stanek et al. 2003; Malesani et al. 2004; Woosley & Bloom 2006). They are the brightest explosions in the present-day universe, releasing, in a matter of few tens of seconds, a large amount of energy ($\sim 10^{52}$ erg) in the form of a hot, possibly magnetized, outflow. GRBs are able to radiate a large fraction of their energy in the form of photons, with an efficiency sometimes approaching 100% (Zhang et al. 2007).

The commonly accepted model for the dissipation of the jet energy and its conversion into radiation is the internal shock synchrotron model (Rees & Mészáros 1994). In this model, differential velocities within the outflow are dissipated through collisionless shock waves that generate strong magnetic fields, accelerate a population of relativistic electrons, and eventually release synchrotron radiation (e.g., Piran 1999; Lloyd & Petrosian 2000). Internal shocks suffer however from poor efficiency (Kobayashi et al. 1997; Lazzati et al. 1999; Spada et al. 2000), being capable of radiating only a few percent of the total energy in the outflow.

In their early evolution, the ouflows of long-duration GRBs interact strongly with the cold and dense material of their progenitor star (MacFadyen & Woosley 1999; Aloy et al. 2000; Zhang et al. 2003, 2004). The interaction strongly modifies the dynamics of the jet, while it is still inside the star. Evaluating the effects of the jet–star interaction at larger scales, when the jet is expanding in the circumstellar material, is of fundamental importance, since a change in the jet dynamics can profoundly affect our understanding of the dissipation and radiation processes at play in the prompt phase of GRBs (Rees & Mészáros 2005; Ghisellini et al. 2007).

Here we present the results of a hydrodynamic simulation that follows a GRB jet out to 65 stellar radii, where the jet material becomes transparent to radiation. Our calculation shows that the interaction of the jet material with the star profoundly affects the subsequent evolution of the jet, generating continuous dissipation through transverse collimation shocks.

This Letter is organized as follows: in Section 2 we present the numerical model adopted for the jet and the progenitor star, in Section 3 we present our result and compute light curves, and in Section 4 we discuss our findings.

2. NUMERICAL MODEL

We considered a 16 solar-mass Wolf–Rayet progenitor star, evolved to pre-explosion (Model 16TI; Woosley & Heger 2006). The jet was introduced as a boundary condition at a distance of 10^9 cm from the center of the star, with a total luminosity $L_{\rm jet} = 5.33 \times 10^{50}$ erg s^{-1}, an initial opening angle $\theta_0 = 10^\circ$, an initial Lorentz factor $\Gamma_0 = 5$, and a ratio of internal over rest-mass energy $\eta_0 = 80$, allowing for a maximum Lorentz factor of $\Gamma_\infty = \Gamma_0\eta_0 = 400$, reachable in the case of complete, non-dissipative acceleration. The jet evolution was computed with the special-relativistic hydrodynamic code FLASH (Fryxell et al. 2000).

Figure 1 shows density images from three frames of the simulation at $t = 7.7$ s, $t = 30.7$ s, and $t = 80.7$ s. The upper panel shows the collimating power of the stellar material. The jet that was injected with an opening angle of 10° is squeezed into a 2° opening angle, with the typical sausage shape due to the presence of strong tangential collimation shocks (Morsony et al. 2007). This simulation extends into a box 10 times bigger than any previously performed in a single run and was run for 150 s. The maximum spatial resolution along the jet axis was 4×10^6 cm, while the maximum spatial resolution in the outer jet was 2.5×10^8 cm. In the central and bottom panels, it is possible to see that the jet remains affected by the shocks out to many stellar radii (20 in the central panel and about 60 in the bottom panel).

3. PHOTOSPHERIC EMISSION AND LIGHT CURVES

A zoom around the jet region in the last panel of Figure 1 shows the effect of the interaction of the outflow with the progenitor material more quantitatively (Figure 2). The head of the jet shows shocks whose normal is parallel to the jet axis and propagate along the jet (similar to internal shocks or to the scenario of reborn fireballs; Ghisellini et al. 2007), while the

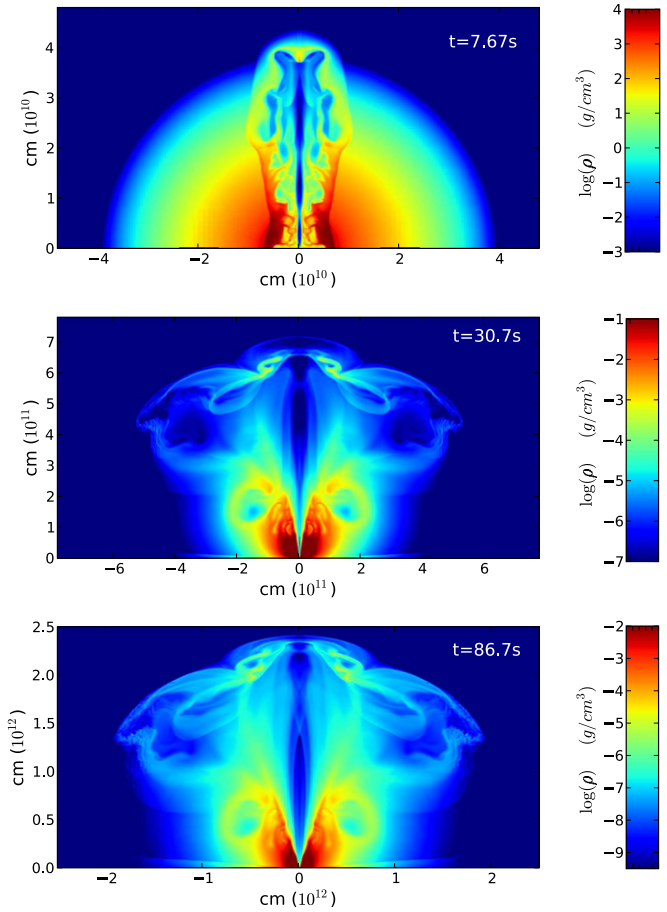

Figure 1. Stills from our simulation of a GRB jet expanding through a 16 solar-mass Wolf–Rayet progenitor star. The jet initially bores a hole in the stellar material (upper panel) and subsequently evolves out to 20 stellar radii (middle panel) and eventually to 60 stellar radii (lower panel). The images show logarithmic comoving density, with the density color scale specified in the right column. The density of the jet in the last panel is sufficiently low for photons to escape to infinity, and the photospheric component of the GRB light curve can be directly computed.

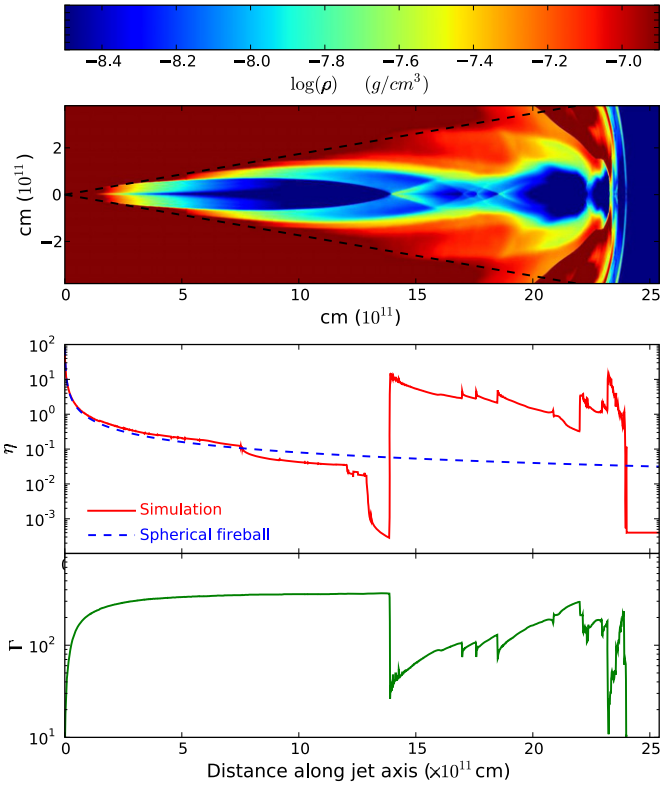

Figure 2. Enhanced dissipation due to shock activity at large radii. This figure is a zoom of the jet region of the lower panel of Figure 1. The figure shows logarithmic comoving density with a color scale enhanced to highlight the shock structure that forms along the jet. Dashed lines show the projected opening angle of the jet for a free expansion, in which the jet keeps the opening angle with which it was injected ($\theta_0 = 10^\circ$). The outer part of the jet, on the right in the image, shows a structure of mainly parallel shocks, in which the normal to the shock front is parallel to the jet axis and to the flow velocity. The intermediate portion of the jet shows instead a structure dominated by tangential collimation shocks. Finally, the inner part of the jet, on the left in the image, shows a more relaxed structure, due to the progressive disappearance of the stellar progenitor's collimating power. The middle panel shows the ratio of the internal energy density to the rest-mass energy density along the jet axis. The blue line shows the prediction for a freely expanding fireball (a conical jet), while the red line shows the results of our simulation. The effect of shocks and a rarefaction wave (at about 1.4×10^{12} cm) are clearly identifiable. The bottom panel shows the Lorentz factor along the jet spine.

part of the jet behind the head is characterized by tangential shocks that propagate from the side of the jet to its axis and vice versa. The middle panel shows the ratio of the internal energy to the rest-mass energy. The dashed blue line shows the theoretical prediction for a freely expanding outflow, neglecting the effect of the interaction with the progenitor material. In that case, $\eta = \eta_0(R_0/R)$, where η_0 is the ratio of internal to rest energy when the jet is released at a radius R_0. The red line shows the result of our simulation along the jet axis. Note that the horizontal scales are equal among panels and the one-to-one correspondence between the shocks and the increases in internal energy. The internal energy dominates over the rest-mass energy much farther out than the simple theory predicts, being ~400 times larger in the region between $R = 1.5 \times 10^{12}$ and $R = 2.5 \times 10^{12}$ cm. The bottom panel of Figure 2 shows the Lorentz factor along the jet spine.

The opacity for Thompson scattering of a relativistically moving medium is (Abramowicz et al. 1991)

$$\tau(R,t) = \sigma_T \int_R^\infty \Gamma(1 - \beta\cos\theta_v) n' dr, \qquad (1)$$

where the comoving density n', the Lorentz factor Γ, and the angle between the line of sight and the velocity of the fluid (θ_v) are evaluated at a laboratory time $t_{\rm lab} = t_{\rm lab,0} + R/c$, where $t_{\rm lab,0}$ is the laboratory time at which the photon is released at a radius R. The photosphere is defined as the radius $R_{\rm phot}$ for which $\tau(R,t) = 1$.

Knowing the photospheric radius as a function of time and angle, we computed the light curve by integrating a thermal spectrum over the angular direction at the comoving temperature boosted by relativistic effects:

$$L = \frac{ac}{2} \int_0^{\pi/2} \frac{T'^4 R^2 \sin(\theta) d\theta}{(1 - \beta\cos\theta_v)^2}, \qquad (2)$$

where $a = 7.56 \times 10^{-15}$ erg cm^{-3} K^{-4} is the radiation constant and T' is the comoving radiation temperature, which is derived from the pressure as $T' = (3p/a)^{1/4}$. Results are shown in Figure 3. The photospheric light curve (Panel a) shows an intensity and a temporal evolution fairly similar to observed GRBs.

It is worth noting here that the jet material is fully ionized and opacity is mainly provided by Thompson scattering, with a minor contribution from free–free processes. In such conditions,

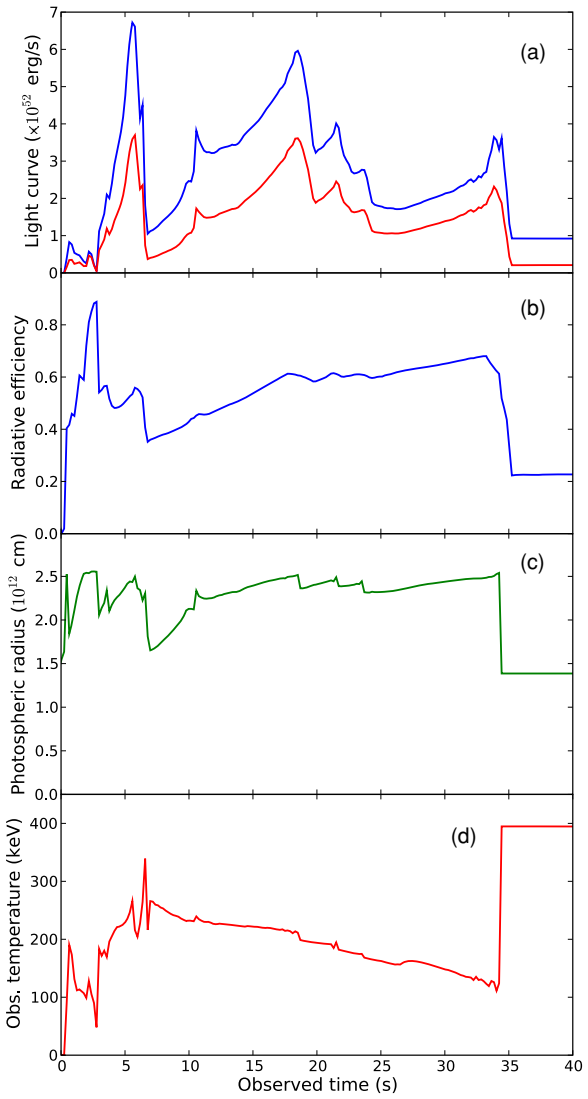

Figure 3. Photospheric light curve and properties for an on-axis observer at infinity. Panel (a) shows the total light curve (blue line) and the photospheric component (red line) for an observer lying along the jet axis. Panel (b) shows the photospheric fraction, i.e., the fraction of the total energy that is released at the photosphere. This represents a lower limit to the radiative efficiency since additional dissipation and radiation of non-thermal photons can take place beyond the photosphere. Panel (c) shows the radius of the photosphere that contributes photons at time t along the jet axis. Finally, Panel (d) shows the observed temperature of the photospheric component in keV. The predicted temperature is strikingly similar to the typical peak frequency of observed GRBs.

the spectrum is slightly broader than a blackbody (Goodman 1986), but has the same peak frequency and fairly similar asymptotic behavior. In addition, a population of non-thermal particles could be present due to the shocks that keep the photosphere hot. Such non-thermal electrons would create a non-thermal tail at high energies due to inverse Compton scattering. However, if the high-energy tail extends to comoving energies $h\nu' > 511$ keV, photon–photon interaction may become relevant as a source of opacity for high-energy photons as well as a source of electron–positron pairs that could alter the location of the photosphere (e.g., Mészáros et al. 2002). The details of the opacity calculation depend on the assumed non-thermal tail of the spectrum. In this Letter, we concentrate on the thermal emission from the photosphere and therefore the pairs are not an issue. The explanation of GRB spectra extending to energies larger than $h\nu \sim 50(\Gamma/100)$ MeV require a more detailed calculation and assumptions on the spectrum of non-thermal particles that go beyond the scope of this Letter.

The kinetic energy remaining in the jet beyond the photosphere was used to evaluate the minimum radiative efficiency. It is about 50%, with an average of 56% in the first 40 s of the light curve (see Figure 3, Panel b). Figure 3 (Panel c), shows the photospheric radius along the jet axis as a function of time, while Panel (d) shows the observed peak of the photospheric emission in keV. The peak of a few hundred keV seen in the simulation is typical for long-duration GRBs (Kaneko et al. 2006). Note that at times longer than ∼35 s the jet enters the "unshocked jet phase," as discussed in Morsony et al. (2007). In this phase, the photospheric efficiency drops since tangential shocks are absent in the "unshocked" phase.

4. DISCUSSION

Our simulation shows that the interaction of the relativistic outflow with the progenitor material in long-duration GRBs has effects that are important well after the jet has left the star. The jet does not cool and has a very bright photosphere yielding a high radiative efficiency in the prompt phase. In addition, the photospheric component is quasi-thermal (Rees & Mészáros 2005; Thompson et al. 2007; Pe'er 2008) offering an explanation for the hard X-ray spectra in the early phase of GRBs, which is inconsistent with synchrotron (Preece et al. 1998; Ghisellini et al. 2000). Thermal components have been detected recently in BATSE spectra (Ghirlanda et al. 2003, 2007; Ryde 2005; Ryde & Pe'er 2008) and the Fermi gamma-ray telescope will soon give us a wideband view of the bursts' prompt emission. Non-thermal components can be added to the spectrum as a result of the reprocessing of photospheric emission and of additional dissipation due to the large inhomogeneities in the jet Lorentz factor (see the bottom panel of Figure 2). Additional work is however required to assess the capability of this model to explain the very high energy photons observed, e.g., in GRB 080916C (Abdo et al. 2009). Unless an extremely large value of the Lorentz factor of the fireball is assumed ($\Gamma > 10^4$ to explain photons of 10 GeV), photons of GeV energy need to be released at a radius of at least $\sim 10^{15}$ cm (Zhang & Pe'er 2009). Photospheres cannot be located at such large radii, even if the opacity is increased by electron–positron pair production. If the keV to MeV photons of GRB 080916C are from the photosphere, as we argue, a second emission mechanism is required for the GeV component. Kumar & Barniol Duran (2009) argue that the >100 MeV photons observed in GRB 080916C must be produced in the external shock due to their temporal evolution that is different from the one of the keV to MeV photons. In such a scenario, the keV to MeV radiation of GRB 080916C could be photospheric. It is also possible that photons of the photospheric emission are inverse Compton scattered by hot electrons at large radii (heated, e.g., in an internal shock) to produce a high-energy tail in the GeV band.

Our computation has two main limitations. On the one hand, it represents one single case of a jet, with given characteristics, interacting with a given star. It is not straightforward to predict how different would be the photospheric component for a different jet with a different progenitor star. Based on the result of simulations of smaller domain (Figure 4), we can speculate that bigger stars will produce a stronger photospheric component and that the diversity in progenitor population would explain the range of thermal to non-thermal ratios and efficiencies observed in GRBs. Higher luminosity jets are also expected to produce

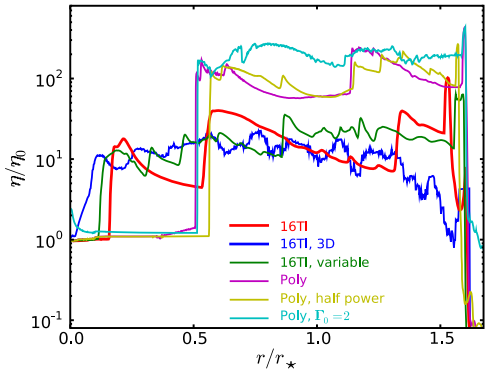

Figure 4. Comparison between the excess internal energy ratio of different jet/progenitor models. The vertical axis shows the ratio between the actual internal to rest-mass energy (η) over the internal to rest-mass energy ratio in a freely expanding jet (η_0). The horizontal axis shows the distance along the jet in units of the progenitor star radius. The reference model discussed in the Letter is shown with the thick red line and labeled "16TI." Model "16TI, 3D" shows an identical physical setup, but computed in three dimensions. Model "16TI, variable" shows a jet with the same average luminosity, but with short timescale variations, expanding in the reference progenitor. Model "poly" shows the reference jet expanding in a bigger star ($r_\star = 10^{11}$ cm) with a polytropic density profile and a total mass of 15 $M_\odot$. Model "poly, half-power" shows a jet with half the luminosity of the reference jet expanding in the poly progenitor. Model "poly, $\Gamma_0 = 2$" shows a jet with an initial Lorentz factor of 2 (compared to $\Gamma_0 = 5$ of the reference jet) propagating through the poly progenitor.

brighter photospheres, since they produce thicker cocoons (Aloy et al. 2000). Mizuta & Aloy (2009) performed a systematic study of jets into a diverse set of progenitor stars, finding that the early jet evolution is largely affected by the structure of the stellar progenitor. On the other hand, the simulation does not have a magnetic component, but is still debated whether the launching and collimation of the jet are due to magnetic effects (e.g., McKinney 2006) or not (see, e.g., Aloy & Obergaulinger 2007). Despite these limitations, our result opens a new window for the understanding of radiation from GRB jets.

We thank the anonymous referee for a careful review that improved the clarity and content of this Letter. We thank Chris Fryer, Ehud Nakar, Asaf Pe'er, Daniel Proga, Felix Ryde, Jay Salmonson, and Bing Zhang for insightful discussions. The software used in this work was in part developed by the DOE-supported ASC/Alliance Center for Astrophysical Thermonuclear Flashes at the University of Chicago. This work was supported in part by NASA ATP grant NNG06GI06G and Swift GI program NNX06AB69G and NNX08BA92G. We thank NCSA and the NASA NAS for the generous allocations of computing time.

REFERENCES

Abdo, A. A., et al. 2009, Science, 323, 1688
Abramowicz, M. A., Novikov, I. D., & Paczynski, B. 1991, ApJ, 369, 175
Aloy, M. A., Müller, E., Ibáñez, J. M., Martí, J. M., & MacFadyen, A. 2000, ApJ, 531, L119
Aloy, M. A., & Obergaulinger, M. 2007, in Rev. Mex. Astron. Astrofis. Conf. Ser. 30, Circumstellar Media and Late Stages of Massive Stellar Evolution, ed. G. García-Segura & E. Ramirez-Ruiz (Mexico City: UNAM), 96
Fryxell, B., et al. 2000, ApJS, 131, 273
Ghirlanda, G., Bosnjak, Z., Ghisellini, G., Tavecchio, F., & Firmani, C. 2007, MNRAS, 379, 73
Ghirlanda, G., Celotti, A., & Ghisellini, G. 2003, A&A, 406, 879
Ghisellini, G., Celotti, A., Ghirlanda, G., Firmani, C., & Nava, L. 2007, MNRAS, 382, L72
Ghisellini, G., Celotti, A., & Lazzati, D. 2000, MNRAS, 313, L1
Goodman, J. 1986, ApJ, 308, L47
Hjorth, J., et al. 2003, Nature, 423, 847
Kaneko, Y., Preece, R. D., Briggs, M. S., Paciesas, W. S., Meegan, C. A., & Band, D. L. 2006, ApJS, 166, 298
Kobayashi, S., Piran, T., & Sari, R. 1997, ApJ, 490, 92
Kumar, P., & Barniol Duran, R. 2009, arXiv:0905.2417
Lazzati, D., Ghisellini, G., & Celotti, A. 1999, MNRAS, 309, L13
Lloyd, N. M., & Petrosian, V. 2000, ApJ, 543, 722
MacFadyen, A. I., & Woosley, S. E. 1999, ApJ, 524, 262
Malesani, D., et al. 2004, ApJ, 609, L5
McKinney, J. C. 2006, MNRAS, 368, 1561
Mészáros, P., Ramirez-Ruiz, E., Rees, M. J., & Zhang, B. 2002, ApJ, 578, 812
Mizuta, A., & Aloy, M. A. 2009, ApJ, 699, 1261
Morsony, B. J., Lazzati, D., & Begelman, M. C. 2007, ApJ, 665, 569
Pe'er, A. 2008, ApJ, 682, 463
Piran, T. 1999, Phys. Rep., 314, 575
Preece, R. D., Briggs, M. S., Mallozzi, R. S., Pendleton, G. N., Paciesas, W. S., & Band, D. L. 1998, ApJ, 506, L23
Rees, M. J., & Mészáros, P. 1994, ApJ, 430, L93
Rees, M. J., & Mészáros, P. 2005, ApJ, 628, 847
Ryde, F. 2005, ApJ, 625, L95
Ryde, F., & Pe'er, A. 2008, ApJ, submitted (arXiv:0811.4135v1)
Spada, M., Panaitescu, A., & Mészáros, P. 2000, ApJ, 537, 824
Stanek, K. Z., et al. 2003, ApJ, 591, L17
Thompson, C., Mészáros, P., & Rees, M. J. 2007, ApJ, 666, 1012
Woosley, S. E. 1993, ApJ, 405, 273
Woosley, S. E., & Bloom, J. S. 2006, ARA&A, 44, 507
Woosley, S. E., & Heger, A. 2006, ApJ, 637, 914
Zhang, B., & Pe'er, A. 2009, ApJL, submitted (arXiv:0904.2943)
Zhang, B., et al. 2007, ApJ, 655, 989
Zhang, W., Woosley, S. E., & MacFadyen, A. I. 2003, ApJ, 586, 356
Zhang, W., Woosley, S. E., & Heger, A. 2004, ApJ, 608, 365